This article citation: Gao Z et al. Drive cycle simulation of high efficiency combustions on fuel economy and exhaust properties in light-duty vehicles. Applied Energy 157 (2015) 762–776, http://dx.doi.org/10.1016/j.apenergy.2015.03.070

Drive cycle simulation of high efficiency combustions on fuel economy and exhaust properties in light-duty vehicles

Zhiming Gao, Scott J. Curran, James E. Parks II, David E. Smith, Robert M. Wagner, C. Stuart Daw, K. Dean Edwards, and John F. Thomas

Oak Ridge National Laboratory
National Transportation Research Center
2360 Cherahala Boulevard
Knoxville, TN 37932

Corresponding author: Zhiming Gao

Email address: gaoz@ornl.gov

Tel: +1-865-946-1339; Fax: +1-865-946-1354

Present address: Oak Ridge National Laboratory
National Transportation Research Center
2360 Cherahala Boulevard
Knoxville, TN 37932

This manuscript has been authored by UT-Battelle, LLC under Contract No. DE-AC05-00OR22725 with the U.S. Department of Energy. The United States Government retains and the publisher, by accepting the article for publication, acknowledges that the United States Government retains a non-exclusive, paid-up, irrevocable, world-wide license to publish or reproduce the published form of this manuscript, or allow others to do so, for United States Government purposes. The Department of Energy will provide public access to these results of federally sponsored research in accordance with the DOE Public Access Plan (http://energy.gov/downloads/doe-public-access-plan).

This article citation: Gao Z et al. Drive cycle simulation of high efficiency combustions on fuel economy and exhaust properties in light-duty vehicles. Applied Energy 157 (2015) 762–776, http://dx.doi.org/10.1016/j.apenergy.2015.03.070

Abstract

Results from computational simulations of fuel economy and engine-out emissions are presented for light-duty conventional and hybrid vehicles powered by conventional and high-efficiency combustion engines, including use of port fuel-injected, lean gasoline direct injection, reactivity controlled compression ignition, and conventional diesel combustion. The results indicate that multimode operation with conventional diesel combustion plus reactivity controlled compression ignition, conventional diesel combustion only, and lean gasoline direct injection has the potential to significantly exceed port fuel-injected fuel economy. In all cases, hybridization is predicted to significantly improve fuel economy by permitting the maximum exploitation of high efficiency engine combustion states. Predicted engine-out emissions vary considerably with combustion mode, with reactivity controlled compression ignition generating the highest carbon monoxide and hydrocarbon emissions. On the other hand, reactivity controlled compression ignition is predicted to generate the lowest emissions of nitrogen oxides. Importantly, lean gasoline direct injection and reactivity controlled compression ignition combustion modes are expected to dramatically decrease exhaust temperatures, especially for reactivity controlled compression ignition, which can potentially limit aftertreatment performance. While all results presented are from simulations, the results provide prediction of important details and trends for advanced vehicles that are currently extremely difficult to experimentally study.

Highlights:

- Vehicles powered with various engine technologies are simulated using map-based models.
- Hybridization improves energy saving and emissions control of lean GDI and RCCI.
- Lean GDI and RCCI combustion modes significantly decrease exhaust temperatures.
- The new U.S. EPA Tier 3 Bin 30 NOx+NMOG emission regulation is challenging.

Keywords: fuel economy, emissions, engine efficiency, hybrid vehicle, drive cycle

1. Introduction

The existing light-duty (LD) vehicle fuel economy regulations require a U.S. fleet average of 35.5 miles per gallon in 2016, increasing to 54.5 miles per gallon by 2025 [1]. Although a comprehensive integration of viable technologies at a vehicle level is necessary, high-efficiency combustion engines will play a critical role in achieving such challenging targets. Most of the current engines used in LD vehicles are spark ignited (SI) gasoline, and a small amount are direct injection (DI) diesel. Port fuel-injected (PFI) SI stoichiometric gasoline engine technology dominates in the current U.S. fleet; however, PFI gasoline engine will have significant problems in meeting the new fuel economy standards. For example, air supply in PFI engines is regulated with a throttle plate, leading to considerable pumping loss due to throttling; furthermore, lower compression ratios employed in PFI gasoline engines produce lower engine efficiencies compared to direct injection systems [2].

Recently, direct gasoline injection (GDI) technology has been increasingly introduced in new model vehicles and is displacing PFI engines [3-6]. GDI gasoline engines have been reported to achieve higher fuel economy over their PFI counterparts, and offer a performance benefit at high load [3-7]. In addition, the same three-way catalyst technology used for PFI engines to control emissions is easily applied for GDI engines operating at stoichiometric air-to-fuel ratios. As one strategy to improve LD vehicle fuel economy, many automobile manufacturers already offer passenger car and LD truck models equipped with smaller displacement, turbocharged GDI engines which replace larger displacement PFI engines [5, 8].

Significant engine studies illustrate that lean GDI engine technology can achieve further improvements in vehicle fuel economy by operating at lean air-to-fuel ratios over significant portions of the engine speed-load range [7, 9-11]. However, lean gasoline exhaust requires complex and costly oxides of nitrogen (NOx) control catalysts due to its high oxygen content which renders the three-way catalyst ineffective for NOx reduction [3, 7]. Both engine and chassis dynamometer measurements also show that lean GDI engines generate more particulate matter (PM) than their PFI counterparts [4, 12-13]; in fact, lean GDI engine PM mass levels exceed those of diesels equipped with diesel particulate filters [5].

Conventional diesel combustion (CDC) engines are attractive for LD applications due to their higher thermal efficiencies. It is well known that diesel engines require complex and expensive lean exhaust aftertreatment systems for NOx and PM emissions control [14-16]. To address aftertreatment costs, studies are exploring innovative combustion strategies which enable higher fuel efficiencies than diesel engines while simultaneously lowering engine-out emissions to reduce aftertreatment costs [17-20]. Such novel combustion modes usually involve flameless or staged fuel combustion and are known as low-temperature combustion (LTC). The LTC strategy has many variants including homogeneous charge compression ignition (HCCI), partially-premixed charge compression ignition (PCCI), and reactivity controlled compression ignition (RCCI) [21-23]. While HCCI is applicable for gasoline-like fuels and PCCI is used for diesel-like fuels, RCCI is an emerging combustion strategy that utilizes in-cylinder fuel blending of low- and high-reactivity fuels (e.g., a diesel-like and gasoline-like fuel in combination) to produce low NOx and PM emissions, while maintaining higher thermal efficiency [18,19,23].

RCCI introduces a low-reactivity fuel (e.g. a gasoline-like fuel) into the cylinder to create an initial well-mixed, in-cylinder charge. Then a high-reactivity fuel (e.g. a diesel-like fuel) is injected directly into the combustion chamber before ignition of the premixed fuel occurs. Therefore, the stratification of equivalence ratio, reactivity, and temperature inside the cylinder can be managed flexibly prior to and during combustion. Consequently, both combustion phasing and cylinder pressure rise rate can be controlled to increase brake thermal efficiency while lowering NOx and particulates [23-24]. By modulating the amount of each fuel and the timing of the high-reactivity fuel, global fuel reactivity as well as the reactivity stratification can be varied with engine speed and load, allowing low-temperature combustion to be stabilized over a wider operating range [25-27]. Experiments have reported that RCCI produces diesel-like brake thermal efficiency at low loads and greater than diesel brake thermal efficiency at high loads with an order of magnitude reduction in engine-out NOx as compared to conventional diesel combustion [28-30].

The potential efficiency and emissions benefits of lean GDI and RCCI have been demonstrated in engine dynamometer experiments. However, limited studies have addressed the impact of these combustion technologies on the fuel economy of vehicles operating over transient driving cycles [31]. In particular, there are no full vehicle experiments having been completed with RCCI to date [18]. In the reported studies, the comparisons between the PFI, lean GDI, CDC, and dual-fuel RCCI engine emissions and fuel economy were not well-addressed for both non-hybrid and hybrid LD vehicles. As these combustion modes span a wide range of fuel reactivity, it is important to understand the distinct benefits and deficiencies of these different combustion modes over transient driving cycles. High-efficiency combustion modes, like lean GDI and RCCI, are typically accessible for a portion of the representative engine speeds and loads demanded in realistic drive cycles. For example, one potential barrier to widespread RCCI utilization is that at higher speeds and loads, the pressure rise rate can become sufficiently high to warrant concern over possible mechanical damage. Thus, it is necessary to constrain RCCI operation to regions of engine speed and load where the pressure rise rate is below a critical value. In cases where the drive cycle requires engine operation outside the RCCI-accessible limits, it is necessary to switch to CDC combustion. Likewise, when the speed and load demands return to the RCCI-accessible region, operation can revert back to RCCI. Moreover, utilization of the LTC-enabled engines in on-road vehicles, particularly hybrid electrical vehicles (HEVs), is significantly constrained by real

driving thermal conditions, such as cold start. Thus, it is critical to characterize their impact on vehicle performance including fuel consumption and emissions control.

This effort compares simulated fuel economy and engine-out emissions from lean GDI, RCCI, CDC, and PFI engines in conventional and hybrid LD vehicles. The simulated vehicles were specified using Autonomie which is a state-of-the art forward-looking simulation package for powertrain development, especially for how to optimize vehicles and their components with regard to fuel consumption, pollutant emissions, and vehicle performance [32], In addition to standard Autonomie features, a previously transient engine model was utilized to account for fuel consumption, engine-out emissions and temperature transients. The engine model is based on experimental, steady-state engine maps combined with a previously published methodology to account for drive-cycle transients [33]. The engine performance maps utilized for PFI gasoline combustion, lean GDI, RCCI, and CDC were constructed from dynamometer measurements of a Saab 9-5 BioPower, 2.0-L, fuel-flexible, turbocharged engine; a BMW 120i, 2.0-L engine; a GM, 4-cylinder, 1.9-L, turbocharged diesel engine; and a modified version of the GM diesel engine, respectively. Since the RCCI operation range does not cover the entire speed and load requirements of the simulated light-duty drive cycles, a multi-mode CDC/RCCI operating strategy is used so that the engine operates in RCCI mode whenever possible but switches to CDC at the highest and lowest engine operating points where RCCI is not feasible. Likewise, the lean GDI operation is supplemented with stoichiometric GDI at higher speeds and loads where lean operation is not feasible. Hybrid vehicle powertrains require significant alteration of the engine speed and load map during a drive cycle; thus, the simulations for hybrid vehicle architectures are especially interesting for the lean GDI and dual-fuel RCCI combustion modes that require a multi-mode strategy due to their limited operation range. Multiple city and highway drive cycles are comprised in the study.

2. Simulation Tools and Assumptions

This section provides an overview of the transient engine component model, engine performance maps, vehicle configurations, and drive cycles used in this study.

2.1. Transient Engine Model

The common approach previously used for vehicle simulations employs steady-state “maps” that give experimental engine-out temperatures and species, as well as fuel consumption, as a function of engine speed and load. Although this approach is highly effective for simulations of steady-state operation, it is difficult to capture the hysteretic effects associated with the more complex transient operation occurring during typical driving conditions such as cold-start and rapid acceleration/deceleration. When engine start/stop events associated with HEVs are included, the modeling problem becomes even more complex. To account for these hysteretic effects, a transient engine-out simulation approach is used to estimate both the temperature and emissions in the engine-out exhaust throughout any specified drive cycle. This methodology was developed previously and is reported in detail elsewhere [33]. Briefly, this approach assumes that engine exhaust temperature and emissions can be estimated by applying dynamic correction factors to steady-state engine maps. These correction factors are modeled as dynamic first-order lags associated with a warm-up index determined from the global heat balance on the engine. Lag parameters are estimated from experimental measurements or based on known engine characteristics. The results reported previously [33] indicate that this methodology can predict the correct variations in engine-out emissions, exhaust temperature, and fuel economy associated with cold- and warm-start conditions for both diesel and gasoline engines under realistic drive-cycle conditions.

The engine model has been updated to account for switching between CDC and RCCI modes, as well as lean and stoichiometric modes. Further the enabling signal for RCCI depends not only on RCCI operation region but also the engine’s preceding thermal condition. Experimental experience with RCCI operation at Oak Ridge National laboratory (ORNL) indicates that it is impossible to successfully initiate RCCI at engine block temperatures below 80°C. Thus, in the engine model, the engine thermal state was quantified with a warm-up index (that represents the degree to which the engine has warmed as a function of the difference between its fully cold and final steady-state operating temperatures). In order to initiate RCCI, a warm-up index of 80% is required, which represents an estimated engine block temperature of 80°C for a steady-state, hot engine block temperature of 95°C and an ambient temperature of 20°C. The authors agree that further experimental studies are required to precisely determine the critical temperature for initiating RCCI in partially heated engines.

2.2. Experimental Engine Data and Performance Maps

ORNL has widely investigated lean gasoline and RCCI-enabled engines. The lean gasoline engine experiments were conducted in a 2.0-L, 4-cyclinder engine with direct injection, which is designated to power a MY2008 BMW 1-series 120i vehicle. The RCCI-enabled engine is a modified 2007 GM, 4-cylinder, 1.9-L turbocharged diesel engine. As benchmarks, both stoichiometric PFI combustion in a Saab 9-5 BioPower, 2.0-L, fuel-flexible, turbocharged engine and CDC in the above GM diesel engine were also evaluated. Table 1 lists these engine specifications. All the measurements follow SAE J1349 Standard. The test instrumentation accuracy for engine power testing is ±0.5% for torque, ±0.2% for speed, ±1.0% for fuel flow, ±0.5kPa for gas pressure, and ±2°C for exhaust temperature, respectively.

Table 1: Specifications of the studied engines.

Engine	Saab	BMW	GM
Year	2007	2008	2007
Capacity (cc)	1985	1995	1910
Stroke (mm)	86	90	82
Bore (mm)	86	84	90.4
Compression ratio	9.5:1	12:1	15:1* or 17:1**
Cylinders	4	4	4
Rated torque	240 N-m @ 3800 rpm	210 N-m @ 4250 rpm	315 N-m @ 4250 rpm
Rated Power	112 kW @ 5500 rpm	125 kW @ 6700rpm	110 kW @ 3950 rpm

* RCCI-enabled; ** CDC-only

2.2.1. Lean GDI

The BMW 2.0-L GDI engine uses a spray guided combustion system design in which the piezoelectric injector is located at the top center of the combustion chamber with a spark plug in close proximity to the injector. The designated injection system allows for ignition as the fuel is being injected, resulting in a shorter mixture formation time and lean operation extended to moderate speeds and loads [4, 34]. The engine was characterized with ultra-low sulfur certification gasoline fuel at ORNL's dynamometer facility. Briefly, lean, stratified operation was calibrated to operate up to 4500 rpm and 55% load as shown in Figure 1. In this lean, stratified combustion mode, gasoline is injected late in the compression stroke close to top dead center creating an ignitable mixture near the tip of the spark plug while the rest of the combustion chamber is very lean and non-ignitable. The injections are followed by multiple spark events to insure ignition. The overall air-fuel equivalence ratio (λ, ratio of actual to stoichiometric air-to-fuel ratio) in the lean, stratified mode ranges from 1.9 to 2.2. In the adjacent region of the map at higher loads (i.e., 55-75% load), more fuel is required to meet the torque requirement so a lean, homogeneous combustion mode with additional stratification (referred to as lean homogeneous in [34]) is employed. In this mode, a portion of the fuel is injected during the intake stroke creating a well-mixed, lean, homogeneous mixture, and additional fuel is then injected late in the compression stroke followed by multiple spark events. The overall λ in the lean, homogeneous mode ranges from 1.3 to 1.7. Outside the lean operation range, at high engine speeds and loads, the engine operates in a stoichiometric, homogeneous combustion mode (i.e., λ=1) [34]. In this mode, a portion of the fuel is injected during the intake stroke, and a second, smaller injection occurs early in the compression stroke creating a well-mixed, homogeneous mixture preceding a single spark event occurring close to top dead center. Lean GDI operation lowers engine-out exhaust temperatures relative to stoichiometric operation.

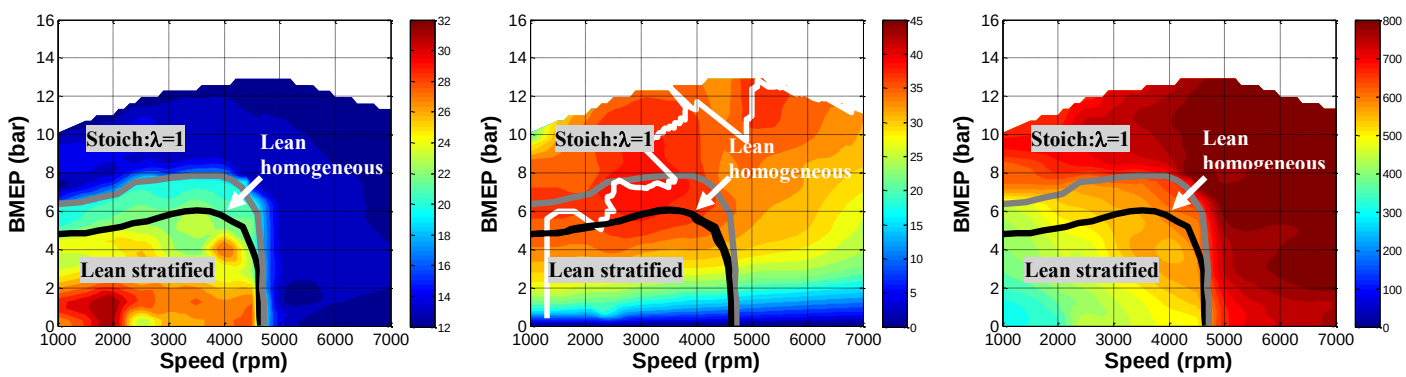

(a) Air/fuel ratio (-) (b) Engine efficiency (%) (c) Exhaust temperature (°C)

Figure 1: Steady-state air/fuel ratio, engine efficiency and exhaust temperature performance maps for BMW 2.0-L engine. The white curve is the optimized engine efficiency per engine power level across the map (b).

The experimental data used to generate the steady-state maps for this engine were collected during vehicle operation on a chassis dynamometer. Engine-out emissions were measured using emission analyzers including: heated chemi-luminescence with ±5ppm accuracy for NOx, non-dispersive infrared with ±0.1% accuracy for Carbon monoxide (CO), Carbon dioxide (CO_2) and paramagnetic for oxygen (O_2) on chilled exhaust, and heated flame ionization detector with ±2.0ppm accuracy for hydrocarbons. Additional detailed information about the experimental setup and generation of the engine data can be found in Chambon et.al. [4] and Prikhodko et al [34].

2.2.2. Dual-fuel RCCI

The experimental data used to generate the RCCI maps for this study were obtained from the modified GM engine with the original pistons replaced by open-bowl pistons which have a lower surface area and provide a lower compression ratio (15.1 versus 17.1 for the stock pistons) [35-37]. The intake manifold has been modified to incorporate extended-tip, narrow spray-angle, port-fuel injectors for the low-reactivity fuel supply while the high-reactivity, direct injection fueling system was left unchanged. Moreover, the stock engine control unit was replaced with a full-pass DRIVVEN control system which allows simultaneous control of the port- and direct-fuel injection systems as well as all other engine parameters. In-depth discussion of the RCCI engine can be found in Curran, et al. [29].

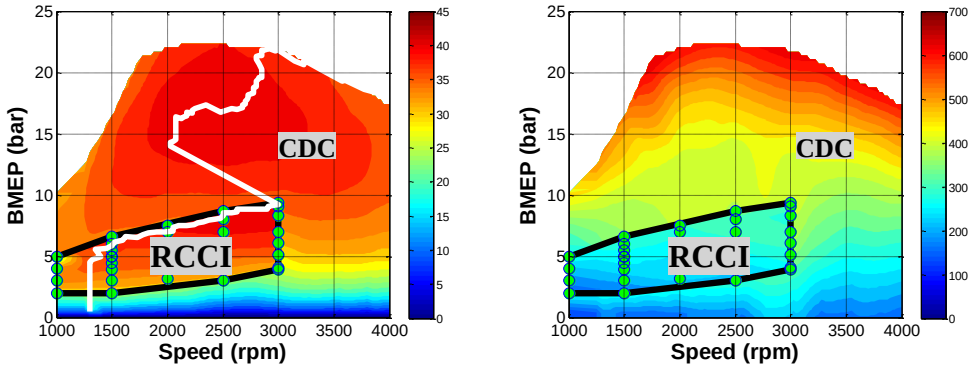

(a) Engine efficiency (%) (b) Exhaust temperature (^{o}C)

Figure 2: Steady-state engine efficiency and exhaust temperature performance maps for the GM, 2.0-L diesel engine operating in RCCI. The white curve is the optimized engine efficiency per engine power level across the map (a).

The DI fuel flow was measured with a MicroMotion Coriolis fuel meter with ±0.1% of flow rate accuracy, while the PFI fuel flow was measured using a Max Machinery 710-213 positive-displacement, volumetric flow measurement system with ±0.2% of flow rate accuracy,. Exhaust temperature was measured with a standard K-type thermocouple with ±2°C measurement error. A heated flame ionization detector measured total unburned hydrocarbons (THC) with ±2.0ppm accuracy, and NOx was measured with a chemi-luminescence detector with ±0.5% measurement accuracy. CO and CO_2 were measured with non-dispersive infrared instruments with ±0.1% accuracy. Intake and exhaust O_2 was measured by a paramagnetic detector with ±1% accuracy. An AVL 415S smoke meter was used to measure filter smoke number (FSN) with the resolution of 0.001 FSN or 0.01 mg/m³ [36-37].

The low- and high-reactivity fuels for RCCI operation were an E30 gasoline/ethanol blend with an anti-knock index (AKI) of 92.1 and a 100% 2007 certification Ultra Low Sulfur Diesel (ULSD) fuel, respectively. The E30 was splash blended with 30% anhydrous ethanol and 70% 87 AKI gasoline containing no ethanol. The ethanol blend is used to improve high-load RCCI performance [13]. To avoid severe engine mechanical damage, two self-imposed constraints for RCCI operations were added to the engine control: (1) maximum in-cylinder pressure rise of 10 bar/deg; (2) maximum 5000 ppm of CO emissions. Otherwise, the engine runs CDC. Figure 2 depicts the boundaries of the CDC operating envelope with the RCCI operating region superimposed. In the figure, the grid points mark the locations where measurements were made to construct the RCCI steady-state emissions and temperature maps.

2.2.3. Stoichiometric PFI and conventional diesel combustion

Stoichiometric PFI combustion was characterized in a Saab 9-5 BioPower, 2.0-L, fuel-flexible, turbocharged engine designed for a 2007 Saab BioPower Sedan [38]. All the measurements were conducted on a chassis dynamometer featuring a twin-roll type (0.55-meter diameter) with an eddy current brake. Conventional emissions measurements were conducted with analyzers from California Analytical Instruments. non-dispersive infrared instruments were used to measure CO_2 and CO. Heated chemiluminescence detectors were used for NOx, and THC and methane were measured with a heated flame ionization detector with a methane cutter. The resolution of these instruments is already discussed above.

Figure 3 shows examples of the stoichiometric PFI engine performance maps. The PFI engine achieves around 30% of the max engine efficiency which is considerably less than the above lean GDI engine (see Figure 1(b)). On the other hand, compared to the lean GDI engine (see Figure 1(c)), the PFI engine produces higher exhaust temperature at lower loads and lower speed.

The CDC performance maps were measured on the 2007 GM, 4-cylinder, 1.9-L, turbocharged diesel engine with a Bosch second-generation common rail fuel injection system, a variable geometry turbocharger, and an electronic exhaust gas recirculation (EGR) valve with high-pressure-loop EGR cooling system [39]. The instruments used in the fuel and exhaust properties measurements of CDC performance are the same as those in RCCI measurements. Figure 4 shows examples of the CDC engine performance maps. The engine employs higher EGR leading to significant NOx emissions reduction at lower loads (see Figure 4(c)). As a penalty, the engine produce a higher CO and HC emissions compared to typical conventional diesel combustion.

This article citation: Gao Z et al. Drive cycle simulation of high efficiency combustions on fuel economy and exhaust properties in light-duty vehicles. Applied Energy 157 (2015) 762–776, http://dx.doi.org/10.1016/j.apenergy.2015.03.070

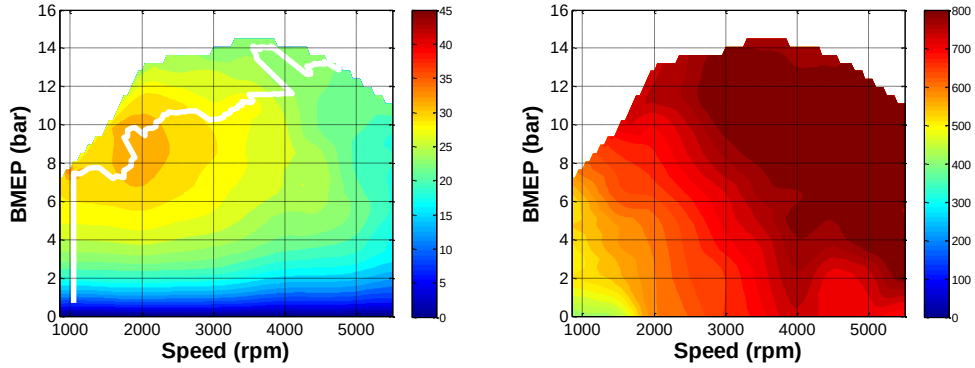

(a) Engine efficiency (%) (b) Exhaust temperature (°C)

Figure 3: Steady-state engine efficiency and exhaust temperature performance maps for SAAB 2.0-L PFI engine. The white curve is the optimized engine efficiency per engine power level across the map (a).

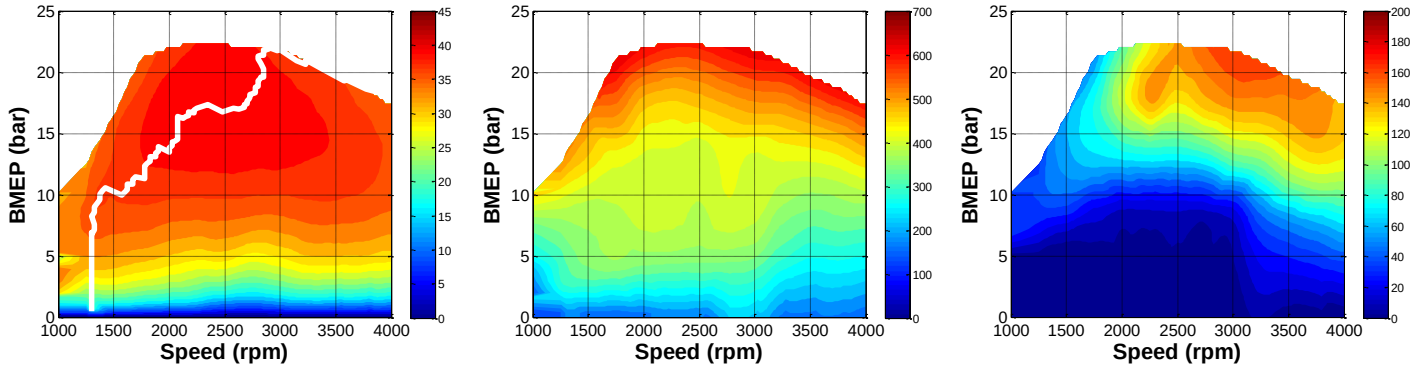

(a) Engine efficiency (%) (b) Exhaust temperature (°C) (c) NOx emissions (g/s)

Figure 4: Steady-state engine efficiency and exhaust temperature performance maps for GM 1.9-L diesel engine operating in CDC mode. The white curve is the optimized engine efficiency per engine power level across the map (a).

2.3. Simulated Vehicle Powertrain Configurations

Both conventional and hybrid powertrain configurations were developed and simulated using Autonomie [32] to account for key components for vehicle powertrain and drivetrain systems, including engine, clutch/torque converter, gearbox, final drive, wheel, chassis, generator, battery, mechanical and electrical accessory loads, as well as motor and high-voltage battery for hybrid powertrain. The simulated conventional powertrain architecture was based on the 1701-kg, conventional, 2012 Ford Fusion powered by a 3.0-L, V6, stoichiometric, gasoline engine and a 6-speed automatic transmission [40]. The simulated hybrid powertrain architecture was based on the 1814-kg, 2010 Ford Fusion hybrid powered by a 2.5-L, stoichiometric, gasoline engine and a power-split planetary gear [40]. Simulations were performed with both powertrain models coupled to each of the map-based engine models discussed above.

Table 2: Specifications of the simulated non-hybrid and hybrid vehicles.

Vehicle	Conventional	Power-split HEV
Engine	PFI/GDI/CDC/RCCI*	PFI/GDI/CDC/RCCI*
Motor	N/A	PM Motor, 78kW@6500rpm, 275V
Battery	Std. ignition battery only	NiMH 275 V/ 1.5 kWh
Transmission/Gear	6-speed manual	Planetary Gear[30/78]
Final drive ratio	3.56	3.56
Wheel radius	0.332 m	0.332 m
Front area	2.25 m^2	2.25 m^2
Rolling resistance coeff	0.007	0.007
Aerodynamic drag coeff	0.27	0.27
Mechanical accessory load	200 W	50 W
Electrical accessory load	100 W	200 W

* Details shown in Table 1.

Table 2 provides specifications for the simulated vehicles. The EV-mode drivetrain in the hybrid vehicle includes a 275-V permanent magnet motor and 1.5-kWh NiMH battery [41]. Since the authors do not have the detailed data for this specific motor and battery, the component models of the Toyota Prius motor and battery provided in Autonomie were resized to simulate the comparable Ford Fusion components. To reasonably account for the different weights of the various drive-train options related to these combustion engines, the weight of engine and other vehicle components were sized based on the peak power demand and recommendations from the ORNL automotive system cost model [42] shown in Appendix A. Thus, the simulated vehicle weight is appropriately adjusted for the chosen engine type and powertrain configuration. Table 2 lists the specifications of these simulated vehicles. The other powertrain components and parameters are assumed to be identical for the two vehicles.

For hybrid vehicle simulations, a charge-sustaining control strategy was adopted to eliminate the need for off-board charging. In the control strategy, the controller commands the engine on if the acceleration demand exceeds specified thresholds, if the motor is saturating, or if power requests are above a threshold value. Otherwise, the engine is off, and all tractive power is supplied by the motor. Motor torque-assist is utilized when the requested tractive torque exceeds engine peak torque at the transient speed. In the controller, the demanded engine torque is determined based on the requested tractive load and battery charging. The power amount for battery charging is determined based on a feedback process as a function of battery state of charge (SOC). During braking, the engine is turned off and the motor acts as a generator to provide power back to the battery. If braking power during regeneration exceeds the battery power charging limit, the former power is considered equal to the latter limit. However, hydraulic braking is demanded if the SOC is above an upper charge threshold, if vehicle or motor speed is below the speed for lower charge thresholds, or if vehicle deceleration is above the maximum regeneration limit. In addition, the optimal brake specific fuel consumption (BSFC) line was developed for each studied engine in order to maximize fuel saving of the power-split configuration. This optimal efficiency line is determined by calculating the speed at which the minimum BSFC occurs for each incremental power level. For addressing impact of cold and warm starts on RCCI-enabled engines, a specific constraint was added allowing the engine to run at optimal CDC efficiencies at cold start and run at optimal RCCI efficiencies during sufficiently warm operations and appropriate loads for RCCI. The engine reverts back to CDC operation if the temperature falls below a critical threshold or the demanded load is outside the RCCI-enabled zone.

Thus, the vehicle models can be utilized to predict vehicle performance over city and highway drive cycles. Briefly, vehicle engine speed and torque or power demands are determined through the simulated vehicles powertrain and drivetrain systems at the given vehicle speed and acceleration/deceleration over a simulated drive cycle with an initial cold- or hot-start, as was extensively reported and reviewed in the open literature [43-44]. Consequently, fuel consumption and engine exhaust properties are predicted using the transient engine model with engine maps as a function of engine speed and torque. To validate that the vehicle models and assumptions provide reasonable accuracy, the simulation results were compared with chassis dynamometer measurements made at Argonne National Laboratory (ANL) using conventional and hybrid Ford Fusion vehicles powered by a 3.0-L and 2.5-L PFI stoichiometric gasoline engines, respectively [40]. Since the authors did not have access to mapping data for these engines, they were simulated by resizing available 2.7-L stoichiometric gasoline engine maps to approximate the 3.0L and 2.5L engines. With these accommodations, corresponding drive cycle simulations were performed and the results were compared to the ANL measurements. Table 3 summarizes the comparison between the simulated fuel economy and ANL's measurements for 3 US EPA drive cycles (see Figure 5) for determining fuel economy of light duty vehicles, including the Urban Dynamometer Driving Schedule (UDDS), Highway Fuel Economy Test (HWFET), and US06 Supplemental Federal Test Procedure. UDDS and HWFET reflect city and highway driving conditions, respectively, while the US06 cycle addresses more aggressive, high-speed driving behavior. The predicted fuel economies shown in Table 3 are reasonably close to the measurements with the largest errors being 5.4% and 7.2% for the conventional and hybrid cases, respectively. Figure 6 further illustrates how the transient fuel consumption and engine speed compared for the hot UDDS cycles. These comparisons reflect that the simulated conventional and hybrid vehicle configurations are reasonably close to the measurements, implying that the basic simulation assumptions concerning the engine and powertrain configuration were indeed reasonable.

Table 3: Comparison between the predicted fuel economies and measurements reported in [40].

Powertrain	Drive cycle unit	Measured FE mpg*	Simulated FE mpg*	Error %
Conventional	Hot UDDS	24.9	25.2	+1.2%
	Hot HWFET	38.9	41.0	+5.4%
	Hot US06	25.7	25.3	-1.6%
Hybrid	Cold UDDS	42.5	45.1	+6.1%
	Hot UDDS	47.5	47.6	<1.0%
	Hot HWFET	48.1	48.3	<1.0%
	Hot US06	32.1	34.4	+7.2%

* 1.0 mpg=0.425 km/L

This article citation: Gao Z et al. Drive cycle simulation of high efficiency combustions on fuel economy and exhaust properties in light-duty vehicles. Applied Energy 157 (2015) 762–776, http://dx.doi.org/10.1016/j.apenergy.2015.03.070

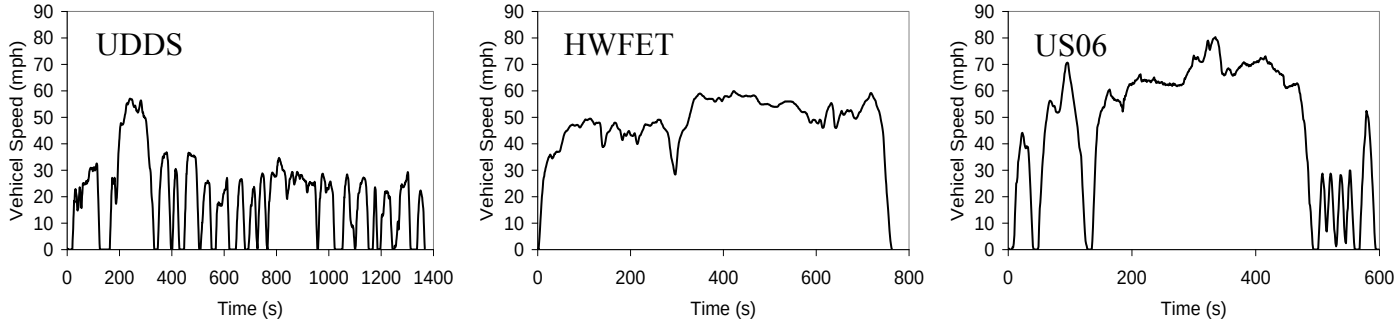

Figure 5: Vehicle speed profiles of UDDS, HWFET, and US06 drive cycles. Vehicle speed units: 1.0 mph=1.61 km/hour.

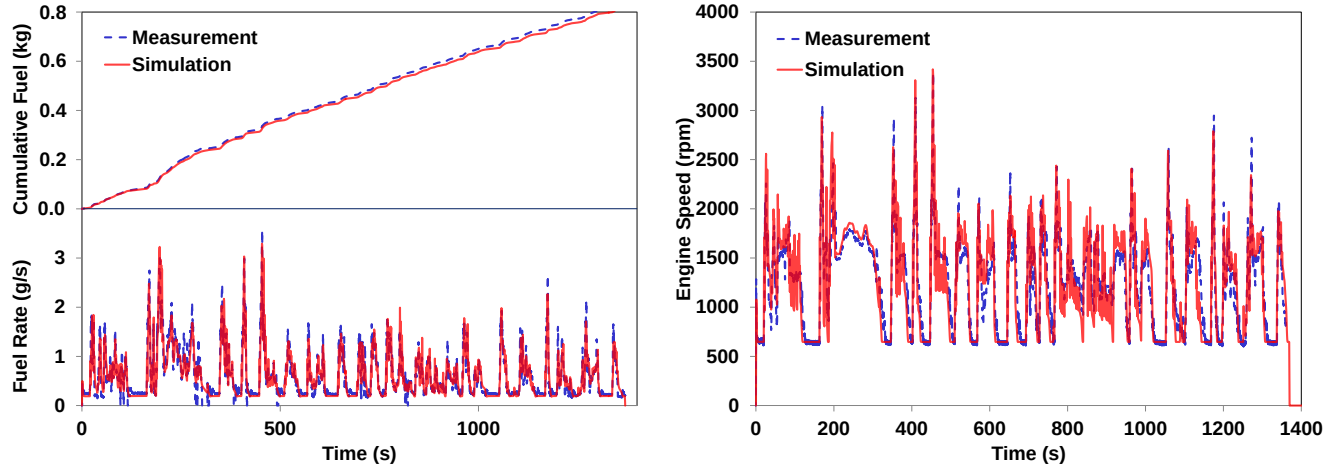

(a) Conventional vehicle

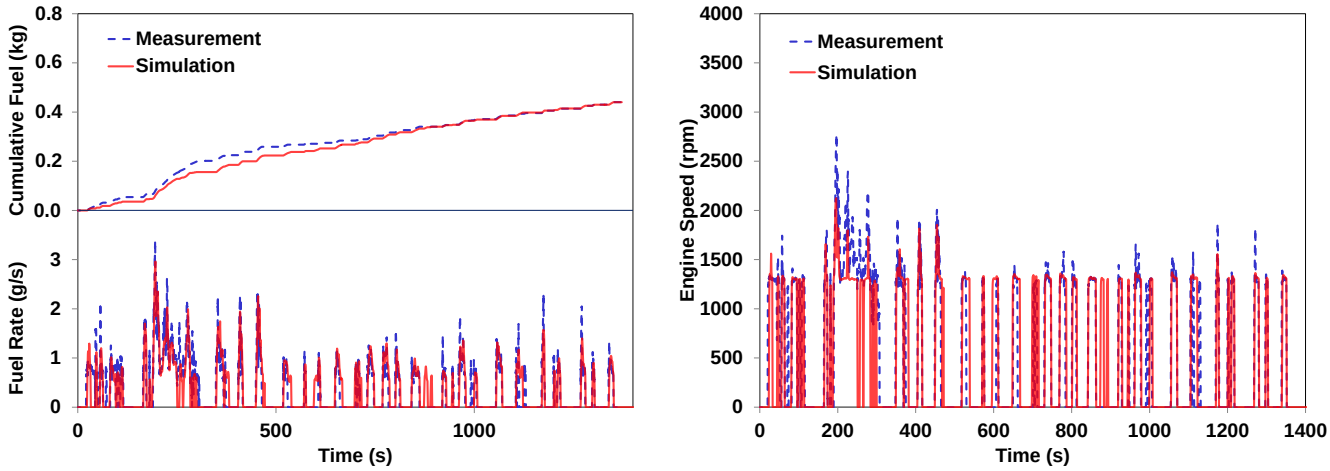

(b) Hybrid vehicle

Figure 6: Comparison of simulated fuel economy and engine speed with the measurements for conventional 2012 Ford Fusion and 2010 Ford Fusion power-split hybrid operating over the hot UDDS.

3. Results

To study the impacts of high-efficiency engines on LD vehicle fuel economy and emissions, the authors used available engine maps from a SAAB 2.0-L PFI engine, a BMW 2.0-L GDI engine, and a GM 1.9-L diesel engine operating with or without RCCI. These 2007-2008 model-year engines including modifications to achieve advanced combustion are indicative of the current and future trends in engine technology. The impact of aftertreatment was not considered in the vehicle simulations, but emissions results from the simulations are valuable in predicting aftertreatment requirements. Each case was simulated using an initial cold-start of 20°C.

This article citation: Gao Z et al. Drive cycle simulation of high efficiency combustions on fuel economy and exhaust properties in light-duty vehicles. Applied Energy 157 (2015) 762–776, http://dx.doi.org/10.1016/j.apenergy.2015.03.070

3.1. Fuel economy simulations

Figure 7 depicts the simulated fuel economies for both the conventional and hybrid vehicles powered by each type of engine. Considering that RCCI involves two fuels (i.e. diesel and E30), diesel equivalent fuel economy is listed for the CDC/RCCI case in order to simplify the analysis. For conventional powertrain cases, Figure 7(a) indicates that the best and worst fuel economies are obtained with CDC/RCCI and PFI, respectively. CDC-only and lean GDI fuel economies are significantly higher than PFI. Compared to CDC-only, CDC/RCCI achieves better fuel economies over all simulated drive cycles. In particular, the benefits grow more substantial for the highway drive cycle. The results are expected because RCCI achieves significantly better engine efficiency than CDC and lean GDI and PFI, as shown in Figures 2 and 4, and confirmed by open literature [13]. For the gasoline engines, lean GDI has 17-23% better fuel economy than PFI. This is primarily due to the fact that lean GDI engine efficiency is considerably higher than PFI over the simulated drive cycles (see Figures 1 and 2), also confirmed by open literature [4]. However, lean GDI fuel economies are still less than CDC-only and RCCI-enabled cases. Importantly, these results do not take into account any fuel consumption required for emission control devices which could alter the comparisons significantly as explained below.

Figure 8 depicts the speed-load points (at 1-second intervals) visited by the conventional vehicle during each drive cycle superimposed over the steady-state brake efficiency map for each engine. These plots reveal that the conventional vehicle spends considerable time in the low-load and low-efficiency region of each engine map over the UDDS and HWFET cycles while significantly operating at the high-load and high speed conditions over the US06 cycle. Compared to stoichiometric PFI shown in Figure 8(a), lean GDI (see Figure 8(b)) achieves considerably better engine efficiency at the same BMEP. Moreover, lean GDI operation (including both lean stratified and lean homogeneous regions) is able to meet 89%-97% of engine operation time and drive distance over the UDDS and HWFET cycles, as listed in Table 4. In detail, most of lean GDI operations in the conventional vehicle stay within the lean stratified region, which meet power demand for 94% of the UDDS and 72% of the HWFET. This confirms again why lean GDI achieves a considerably better fuel economy than PFI. Compared to lean GDI, RCCI shown in Figure 8(c) covers much less engine operation time and drive distance over the city and highway cycles because RCCI is not capable of operating at extra low loads, as seen in Figure 8(c). In addition, cold-start limits RCCI further in transient drive cycles. The white-filled, gray circles in Figure 8(c) represents cold-start, CDC operating points. However, compared to CDC shown in Figure 8(d), the simulated vehicle still enables to operate with the RCCI-enabled region at a certain level of time, which allows the averaged RCCI-enabled engine efficiency better the CDC-only.

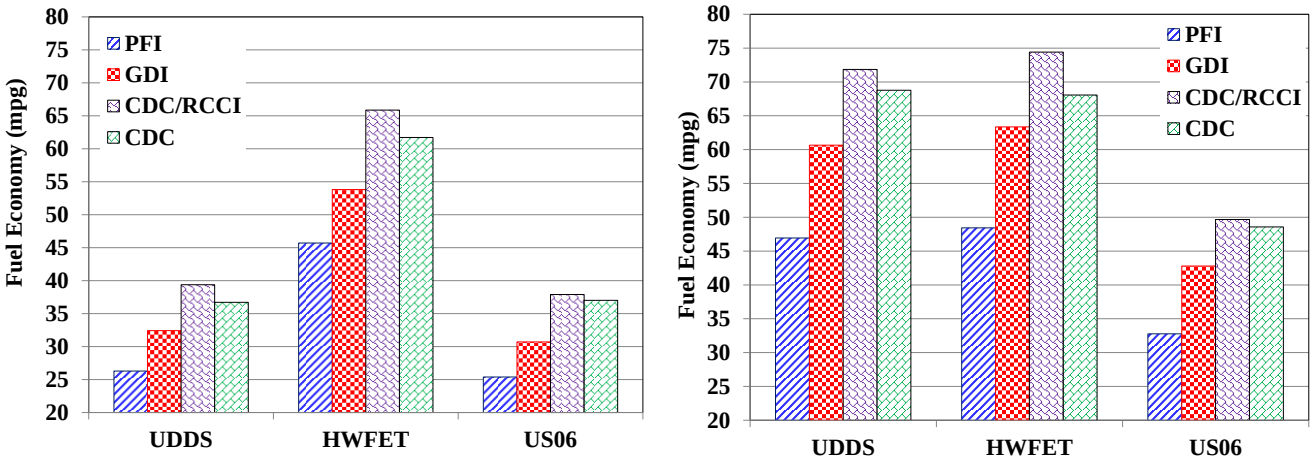

(a) Conventional (b) Hybrid

Figure 7: Fuel economies in the simulated vehicles powered by different combustion engines over various city and highway drive cycles. Fuel economy units: 1.0 mpg = 0.425 km/L.

Table 4: Lean GDI and RCCI drive cycle coverage over various drive cycle simulations.

Combustion	Drive cycles	Powertrain	Drive distance % @ Lean GDI or RCCI	Cycle time%@Lean GDI or RCCI	Engine on time%@Lean GDI or RCCI
Lean GDI*	UDD	Conventional	92.9%	97.1%	97.1%(94.3%@LS, 2.8%@LH)
		hybrid	49.6%	34.3%	99.8%(69.2%@LS, 29.6%@LH)
	HWFET	Conventional	88.8%	89.4%	89.4%(71.9%@LS, 17.5%@LH)
		hybrid	80.6%	77.4%	97.8%(50.9%@LS, 46.9%@LH)
	US06	Conventional	62.1%	72.0%	72.0%(52.5%@LS, 19.5%@LH)
		hybrid	62.3%	51.8%	87.8%(31.7%@LS, 46.1%@LH)
RCCI	UDD	Conventional	42.7%	32.2%	32.2%
		hybrid	42.4%	28.2%	82.3%

This article citation: Gao Z et al. Drive cycle simulation of high efficiency combustions on fuel economy and exhaust properties in light-duty vehicles. Applied Energy 157 (2015) 762–776, http://dx.doi.org/10.1016/j.apenergy.2015.03.070

HWFET	**Conventional**	**63.3%**	**60.2%**	**60.2%**
	hybrid	**76.7%**	**71.6%**	**91.2%**
US06	**Conventional**	**45.3%**	**37.7%**	**37.7%**
	hybrid	**49.7%**	**38.0%**	**65.0%**

*LS: lean stratified; LH: lean homogeneous

For the hybrid powertrain cases, Figure 7(b) shows that all combustion modes achieve better fuel economies than the comparable conventional vehicles, especially for the UDDS cycle. This is expected because UDDS has significant idle time and frequent stop-and-go operation which allows a significant amount of regenerative braking; thus, hybridization can maximize its benefit for vehicle energy savings. Similar to the general trends for the conventional vehicle, the best and worst fuel economies for the simulated hybrid cases are CDC/RCCI and PFI, respectively, and CDC-only and lean GDI are significantly better than PFI. However, lean GDI achieves around 30% higher fuel economies than PFI, which is better than the 17-23% advantage observed with the conventional powertrain. Similarly, CDC-only and RCCI-enabled combustion give 40-48% and 52-54% better fuel economy than PFI, respectively, compared to 35-45% and 44-50% improvement, respectively, for the conventional vehicle. Thus, hybridization can enhance the benefits of lean GDI, CDC-only, and RCCI-enabled engines for energy savings over the discussed drive cycles. Among these engine technologies, CDC/RCCI still achieves the best engine efficiencies over the simulated cycles.

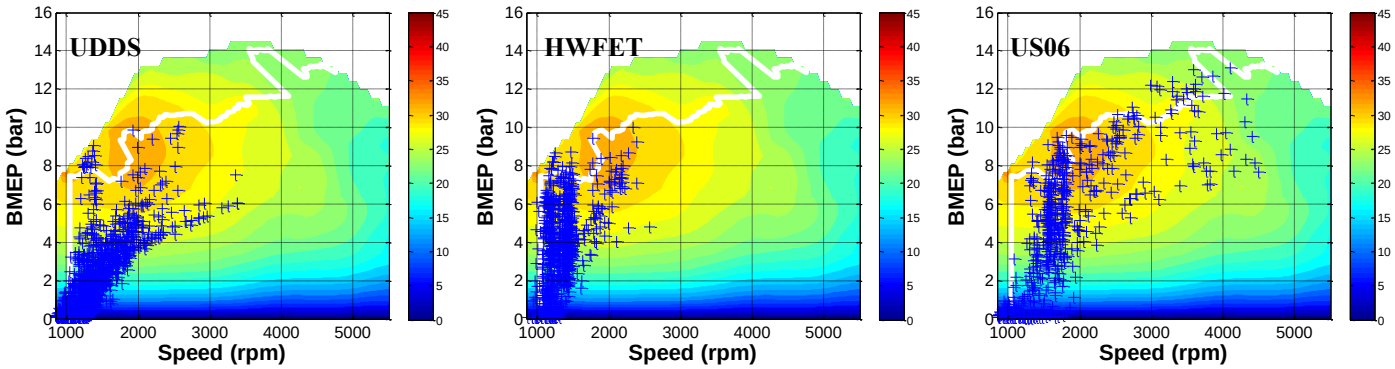

(a) PFI

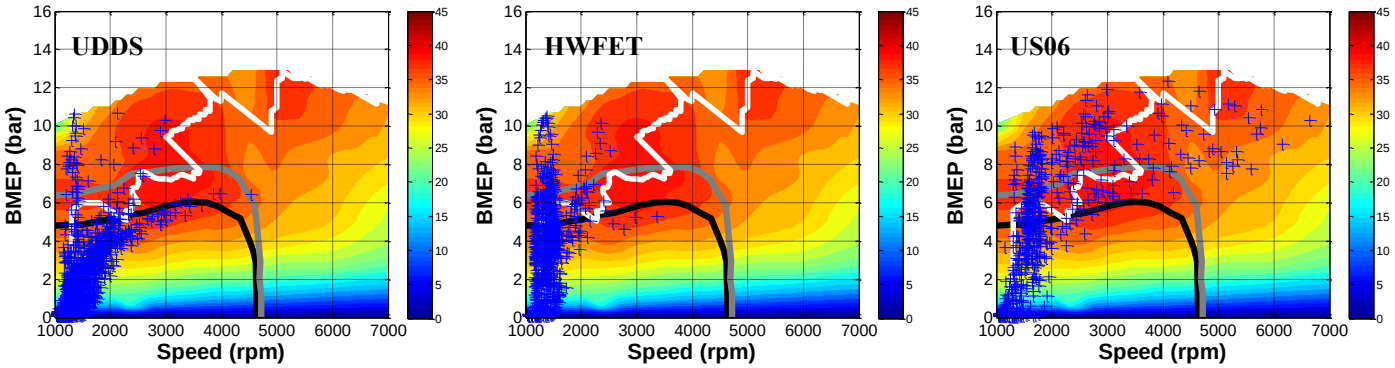

(b) Lean GDI

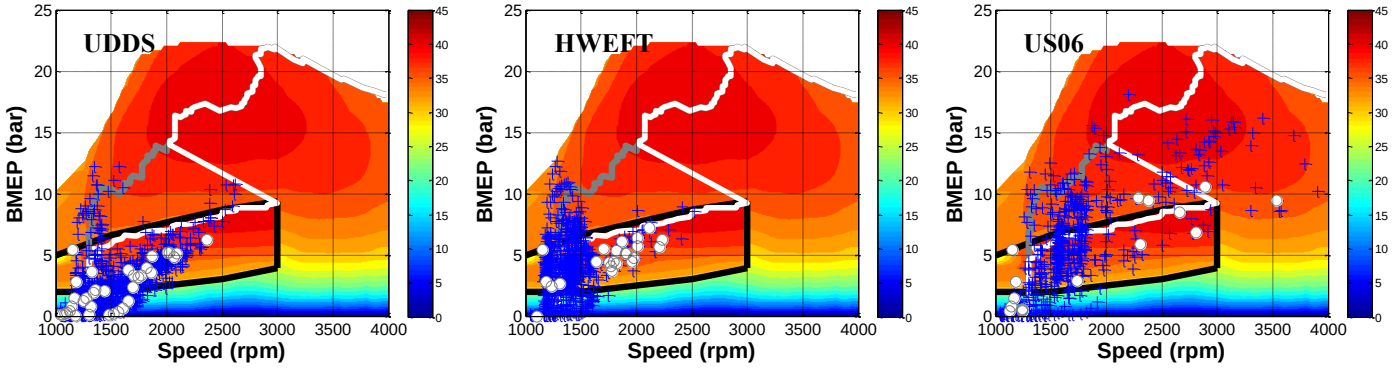

(c) CDC/RCCI

This article citation: Gao Z et al. Drive cycle simulation of high efficiency combustions on fuel economy and exhaust properties in light-duty vehicles. Applied Energy 157 (2015) 762–776, http://dx.doi.org/10.1016/j.apenergy.2015.03.070

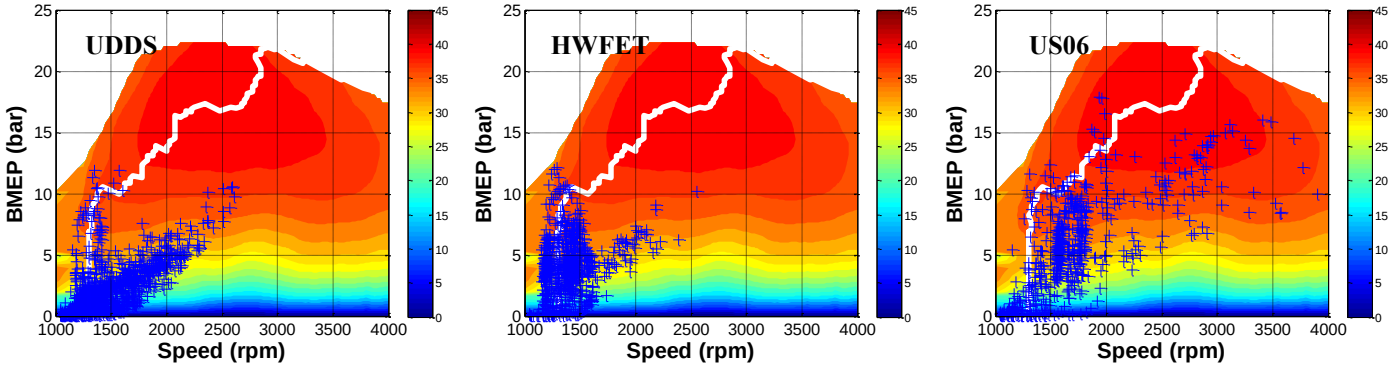

(d) CDC-only

Figure 8: Engine speed-load operating points visited by the simulated conventional vehicle over each drive cycle superimposed on the steady-state brake efficiency map for that engine. Blue crosses represent the engine state at 1-s intervals. The white-filled, gray circles in (c) represent cold-start, CDC operation. Color contours are brake engine efficiency in % and are on the same scale for all plots.

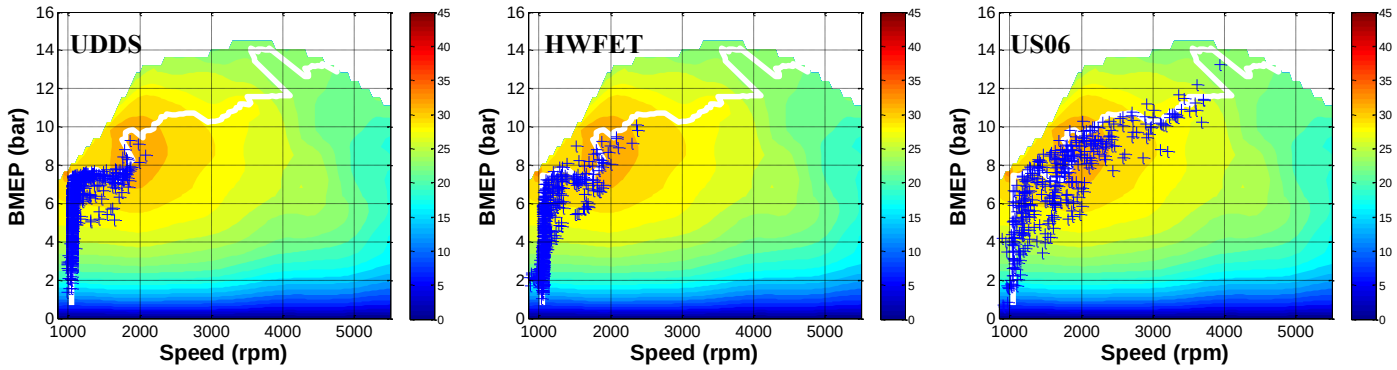

(a) PFI

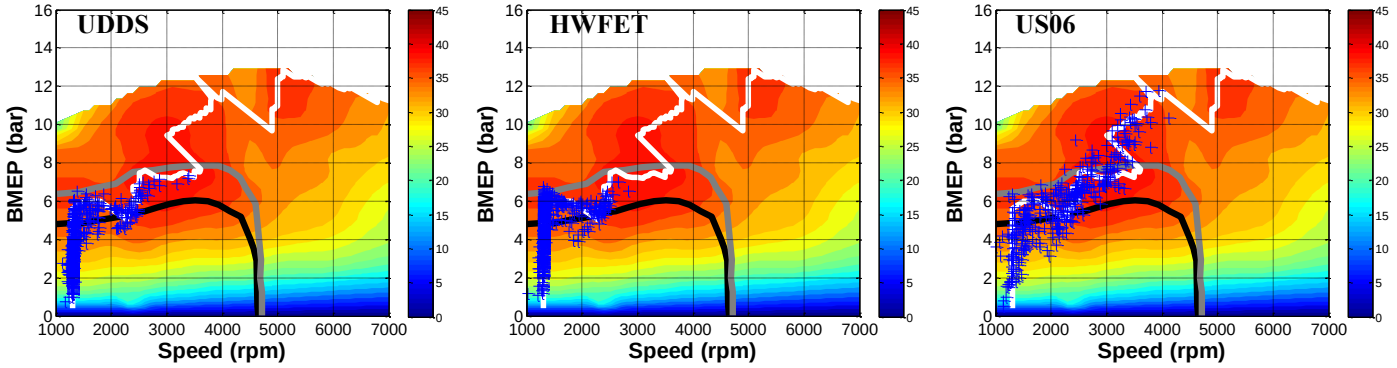

(b) Lean GDI

This article citation: Gao Z et al. Drive cycle simulation of high efficiency combustions on fuel economy and exhaust properties in light-duty vehicles. Applied Energy 157 (2015) 762–776, http://dx.doi.org/10.1016/j.apenergy.2015.03.070

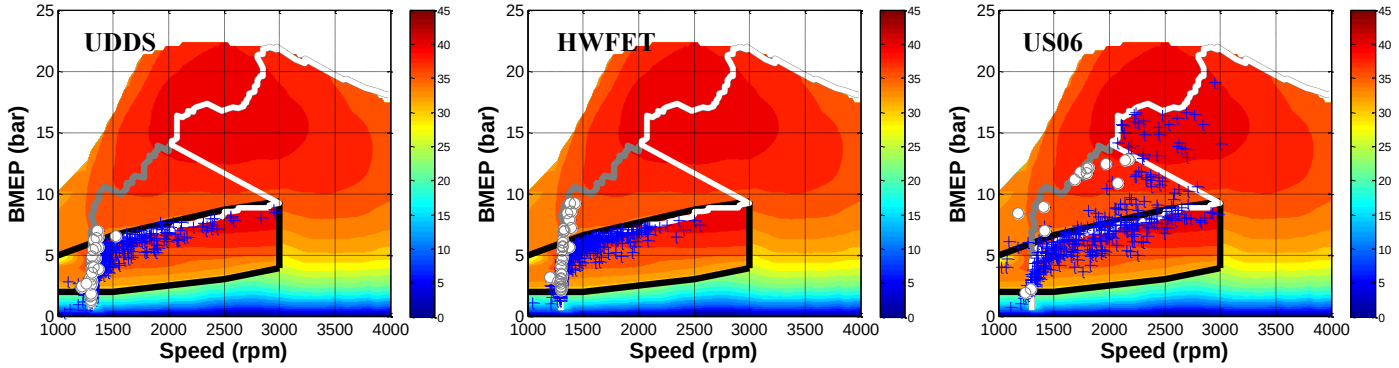

(c) CDC/RCCI

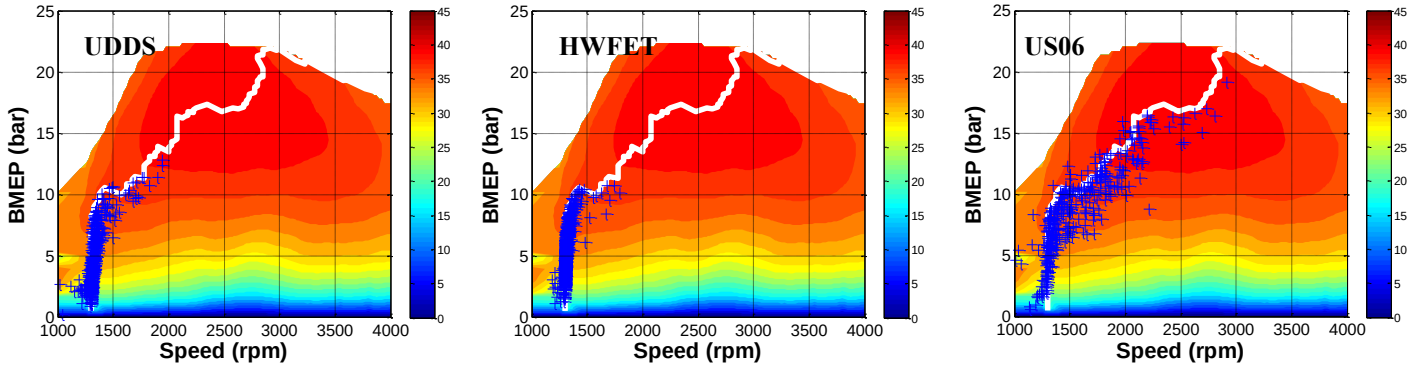

(d) CDC

Figure 9: Engine speed-load operating points visited by the simulated hybrid vehicle over each drive cycle superimposed on the steady-state brake efficiency map for that engine. Blue crosses represent the engine state at 1-s intervals. The white-filled, gray circles in (c) represent cold-start, CDC operation. Color contours are brake engine efficiency in % and are on the same scale for all plots.

Figure 9 illustrates the speed-load points visited by the hybrid vehicle during each simulated drive cycle superimposed over the steady-state brake efficiency map for each engine. Note that for the hybrid vehicle, each engine spends considerable time close to the white curve representing optimal engine power and efficiency across the maps. Moreover, compared to PFI and CDC-only shown Figure 9(a) and 9(d), respectively, hybridization enables lean GDI and RCCI engines to better meet engine power demand (see Figures 9(b) and 9(c), respectively). For example in the lean GDI case, lean operation occurs at a higher percentage of time in the hybrid scenario relative to the non-hybrid case (see Table 4). This occurs even though the cycle time and drive distance percentages of lean GDI operation over the cycles are reduced due to electrical powertrain (motor) assistance. Furthermore, lean GDI is inclined to operate in the lean homogeneous region, instead of the lean stratified region, which gives greater fuel economy benefit as shown in both Table 4 and Figure 9(b). For RCCI, hybridization allows more RCCI operation over the simulated drive cycles. The drive distance and engine-on time percentages with RCCI are significantly increased in the hybrid case (see Table 4). The effect can be clearly observed in Figure 9(c) where the RCCI operation region meets most hybrid vehicle drive conditions over the UDDS and HWFET cycles except for cold-starts (indicate by white-filled gray circles). As mentioned earlier, the cold-start operations ran with an optimal CDC efficiency curve shown with gray color in Figure 9(c). For US06, there are significant high-load and high-speed engine operating points running outside both the lean GDI and RCCI enabled region in their cases; then the vehicle engines switch to the stoichiometric GDI and CDC, respectively. The benefit of lean GDI and RCCI over the US06 could be reduced compared to the UDDS and HWFET cycles.

3.2. Engine-out emissions simulations

The Federal Test Procedure (FTP) cycle is required by the U.S. Environmental Protection Agency (EPA) for emission certification of light-duty vehicles in the United States. The FTP cycle is derived from the UDDS cycle by adding a third phase lasting 505 s identical to the first phase of UDDS but with a hot start. The third phase starts after the engine is stopped for 10 min. Engine-out emissions and exhaust gas temperature results are plotted in Figures 10-12.

As mentioned earlier, PM emissions of RCCI exhaust were measured based on filter smoke number using an AVL 415S smoke meter. The results show (1) the measured FSN of RCCI exhaust is typically very low (i.e. <0.2 [45]) compared to CDC; and (2) more than 95% of the PM emissions are heavy organic compounds, instead of solid soot [45]. Unfortunately there has not been an accurate

correlation established to convert FSN to PM mass for RCCI operation. Thus PM emissions of RCCI exhaust are not plotted in Figures 10 and 11, but the general trend of RCCI on PM emissions is discussed based on previous research results.

Figure 10 compares simulated conventional vehicle drive-cycle engine-out emissions. PM for PFI cases shown in Figure 10 is zero, as PM emissions from PFI engines are generally smaller than measurement error. It is observed from the figure that the engine-out HC/CO/NOx/PM emissions vary significantly with combustion modes. Compared to PFI, lean GDI achieves substantially less NOx and CO emissions while producing higher HC and PM emissions. Recall, however, that lean NOx control is challenging and likely entails fuel consumption or on-board reductant supply (such as urea). As shown in Figure 10, the PM emissions from lean GDI are approximately 5 mg/mile, which is above the PM regulation standard of 3 mg/mile (EPA Tier 3 Bin 30); however, lean GDI PM emissions are still much less than CDC and RCCI cases (see Figure 10). The estimated engine-out CO and HC emissions from RCCI-enabled combustion are markedly higher than CDC-only, but RCCI makes less NOx emissions. Thus, RCCI improves engine fuel economy while reducing NOx emissions slightly. Results reported in literature indicate that RCCI also produces less PM emissions than CDC [37, 45]. A comparison between lean GDI and RCCI emissions illustrates different emission control challenges for these combustion technologies. RCCI has higher CO, HC, and PM emissions but less NOx than lean GDI. Thus, enabling RCCI to meet Tier 3 regulations will require high HC oxidation efficiency by catalysts while lean GDI engines will require high NOx reduction efficiency in lean operation. Since there are many results reporting the emissions control of PFI and CDC [1-3], it is not necessary to discuss them here to avoid lengthy discussions.

The engine-out emissions of the simulated hybrid vehicles are shown in Figure 11. The trend of engine-out emissions from the simulated hybrid vehicles is generally similar to the conventional vehicles. For example, NOx emissions from lean GDI are less than for PFI, but still significantly higher than for CDC and RCCI; RCCI combustion generates the lowest NOx emissions of all. However, compared to the corresponding conventional cases, there are some unique cases where hybridization offers distinct emission advantages. For all hybrid vehicles, the simulated engine-out CO and HC emissions are significantly reduced (see Figures 10-11). Furthermore, hybridization also reduces 78% of NOx, with the potential for significant PM emissions reduction from RCCI in comparison to the conventional vehicle. The reduction of engine-out NOx due to hybridization is dramatic for RCCI and results from minimizing the CDC operation for the RCCI-enabled engine. For lean GDI, hybridization reduces NOx and PM emissions around 20% and 59%, respectively, based on the details from Figures 10-11. Importantly, lean GDI PM emissions in the hybrid case decrease to 1.9 mg/mile which is below the EPA Tier 3 Bin 30 PM standard, thereby avoiding the requirement of filter-based aftertreatment. Thus, hybridization of lean GDI and RCCI greatly impacts NOx and PM emissions as well as corresponding control strategies while improving fuel economy. Hybridization also reduces 30% of PFI NOx emissions. Interestingly for the CDC case, hybridization increases both NOx and PM emissions by 36% and 23%, respectively. For CDC, hybridization does decreases 78% of CO and 76% of HC emissions. Thus, for the CDC case, hybridization does not alleviate any of the NOx or PM emission control challenges but does decrease CO emissions below 1.0 g/mile thus meeting EPA Tier 3 Bin 30 CO regulations without aftertreatment control for CO.

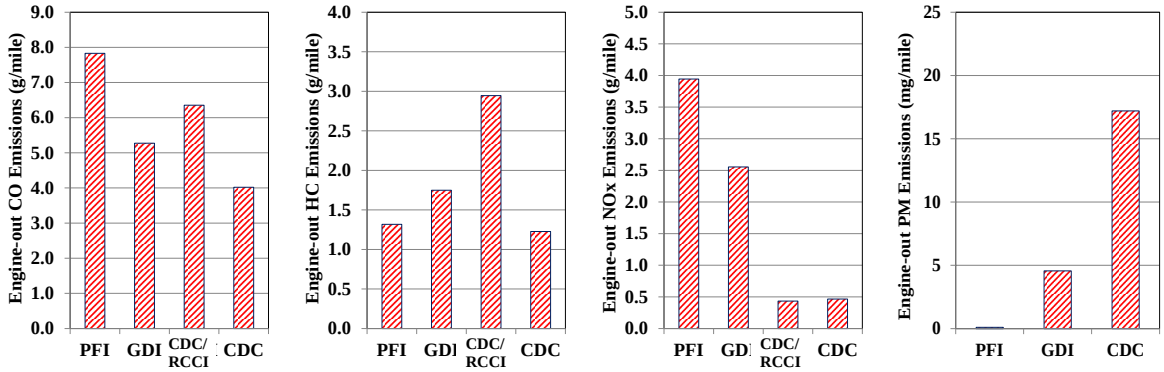

Figure 10: Simulated conventional vehicle engine-out emissions from the PFI, lean GDI, CDC/RCCI and CDC-only engines over the cold-start FTP drive cycle. Emission units: 1.0 g/mile=0.621 g/km.

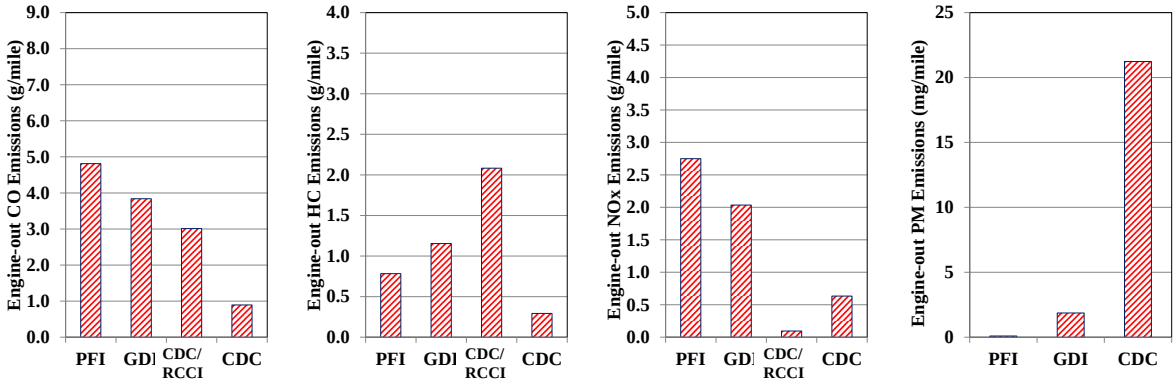

Figure 11: Simulated hybrid vehicle engine-out emissions from the PFI, lean GDI, CDC/RCCI and CDC-only engines over the cold-start FTP drive cycle. Emission units: 1.0 g/mile=0.621 g/km.

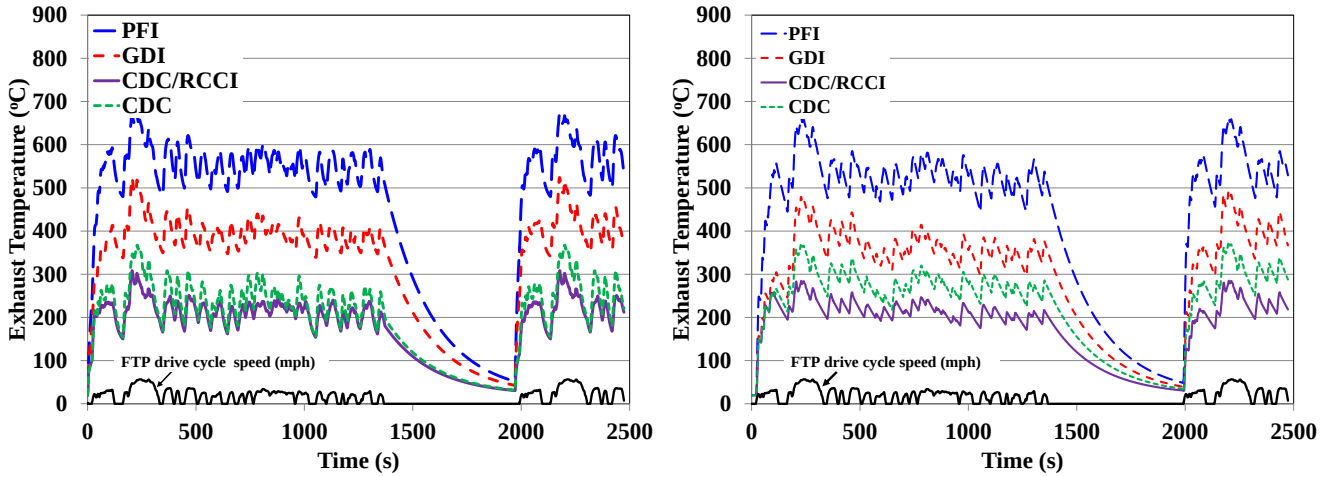

(a) Conventional (b) Hybrid

Figure 12: Simulated exhaust temperatures of the PFI, lean GDI, CDC/RCCI and CDC-only engines in the simulated vehicles under the cold-start FTP cycle.

Figure 12 compares the simulated exhaust temperatures of each engine in both conventional and hybrid vehicles over the cold-start FTP cycle. As shown, exhaust temperatures for the lean GDI gasoline engine are nearly150°C less than the stoichiometric engine but still considerably higher than CDC-only and CDC/RCCI cases. For diesel or diesel-dominated combustion, the RCCI-enabled engine is 50°C -70°C less than the CDC-only engine, and considerable time at exhaust temperatures below 200°C occur over the UDDS cycle. The 200°C level is significant since conventional DOCs have minimal effectiveness for oxidizing HC and CO below this temperature. Thus, the reduced exhaust temperatures may significantly hamper the performance of aftertreatment devices. Finally, compared to non-hybrid vehicles (see Figure 12(a)), the simulated PFI and lean GDI exhaust temperatures (shown in Figure 12(b)) for the hybrid cases are noticeably lower in temperature, but it appears that the CDC-only and RCCI-enabled engine exhaust temperatures are not greatly impacted by hybridization.

4. Implications for Emissions Controls

The above trends imply that combined use of advanced combustion and hybridization should have significant benefits for light-duty fuel economy. However, it is important to also examine how these technologies compare in their achievement of the new U.S. EPA Tier 3 emission standards signed into law in March, 2014 [46]. These standards require the fleet average CO, non-methane organic gases (NMOG)+NOx, and PM emissions to reach 1.0 g/mile, 30 mg/mile, and 3.0 mg/mile (i.e., Tier 3 Bin 30), respectively, by 2025.

Table 5 compares the estimated emission reductions that would be required to meet the new regulations. The most challenging emission category is NMOG+NOx, which requires nearly 99% removal for most cases. In addition, each of the advanced combustion technologies poses different challenges. For example, in the simulated hybrid vehicle, the results depicted in Figure 11 indicate that the total NMOG+NOx emissions from PFI, GDI, and CDC engines are dominated by NOx emissions. On the other hand, the CDC/RCCI engine exhaust is dominated by HCs. Figure 13 further shows that 94%-96% of NOx emissions from PFI, GDI and CDC occur under considerably different exhaust temperature environments, which are 250°C-375°C for CDC only, 300°C-500°C for GDI,

and 400°C-675°C for PFI, respectively. This implies that the aftertreatment technology required is likely to be quite different in each case.

Table 5: Estimated emissions reduction rates required to meet U.S. EPA Tier 3 Bin 30 regulation

Combustion	Drive cycle Unit	CO reduction	NMOG+NOx reduction	PM reduction
PFI	Conventional	87.2%	99.4%	0.0%*
	Hybrid	79.2%	99.2%	0.0%*
Lean GDI	Conventional	81.0%	99.3%	34.3v
	Hybrid	74.0%	99.1%	0.0%*
CDC/RCCI	Conventional	84.2%	99.1%	-
	Hybrid	66.8%	98.6%	-
CDC-only	Conventional	75.1%	98.2%	82.6%
	Hybrid	0.0%*	96.8%	85.9%

* meets the emission standard without aftertreatment.

The three-way catalyst (TWC) technology for PFI engines is highly effective in current vehicles because: (1) exhaust temperatures are well matched to the TWC "light-off" temperature around 400°C, and (2) exhaust chemistry is controlled accurately to enable both oxidation of CO and HC emissions simultaneously with reduction of NOx emissions (via control of combustion to stoichiometric air-to-fuel ratios). Although engine out NOx emissions for lean GDI, CDC, and RCCI are lower than the PFI case, the NOx emission control is much more difficult due to lower exhaust temperatures and excess O_2 in lean exhaust. Both Lean NOx Trap (LNT) and selective catalytic reduction (SCR) catalysts are options for lean NOx emission control, but both approaches require supplemental reductants, increased complexity, and especially for LNTs, added fuel penalties. As mentioned above, total NMOG+NOx emissions from CDC/RCCI are dominated by HC emissions. Compared to CDC only, HC emissions from CDC/RCCI are much higher (see Figures 10 and 11); moreover, a significant amount (66%) of HC emissions from CDC/RCCI are produced between 175°C-250°C (see Figure 13). For a typical oxidation catalyst, a "light-off" temperature for HC oxidation is around 200°C for conventional diesel combustion exhaust. In addition, reported RCCI studies [47] indicate that the combination of higher CO and HC emissions create further difficulty in the oxidation of HCs and typically shift HC "light-off" temperatures from ~200°C up to ~250°C. Due to these issues and the fact that RCCI exhaust temperatures are 50°C-70°C less than CDC exhaust, conventional oxidation catalysts perform worse in RCCI exhaust, confirmed by recent studies [47]. Therefore, it is particularly important to develop improved low-temperature aftertreatment devices to achieve the lower NMOG emissions required to meet the NMOG+NOx standard for RCCI.

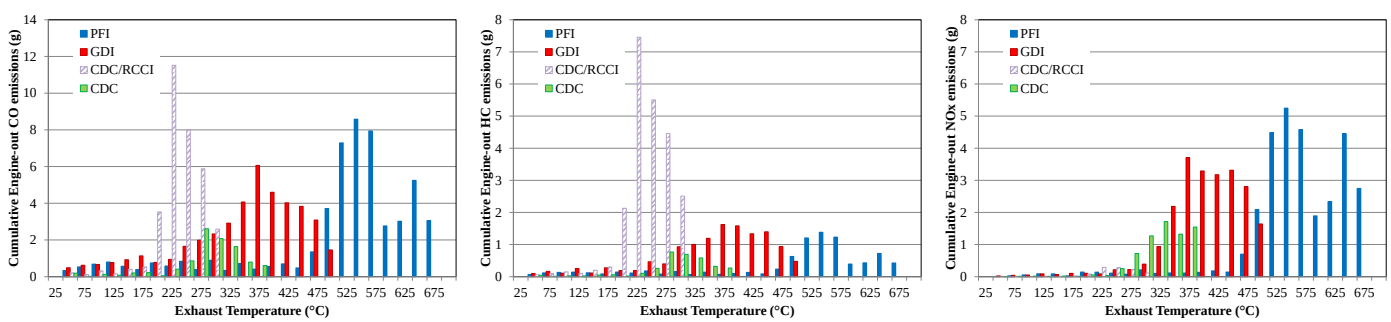

Figure 13: Impact of combustion engine technologies on cumulative engine-out CO/HC/NOx emissions as a function of exhaust temperature in the simulated hybrid under the cold-start FTP cycle.

The control challenges for CO emissions are not as great as for NMOG+NOx emissions. The CDC-only hybrid case can naturally meet the standards without aftertreatment while the other cases require 67-87% removal rates. However, consideration of the impact of CO emissions on the various emission control system components is important. As mentioned above, the combination of significant HC and CO emissions at low temperatures can be problematic for oxidation catalyst control [47]; so, CO can still affect the complete emission control system performance in the specific cases like RCCI, as well as HCCI and PCCI, even if CO is controlled readily to PFI and CDC and GDI.

For PM emissions, the lean GDI hybrid case may naturally meet the PM regulations without PM aftertreatment; yet, the other cases are likely to require 34-86% removal rate. Although RCCI PM results are not shown here, reported experiments indicate significantly less PM emissions from RCCI than CDC [47], and may still require PM reduction aftertreatment technology for achieving 3.0 mg/mile of Tier 3 Bin 30. Current diesel particulate filter (DPF) technology is expected to achieve the necessary level of PM reduction, but the lower PM removal rates required may enable fuel savings due to less frequent filter regeneration. PM emissions from CDC are the highest of all engines shown in Figures 10-11 so that the fuel consumption for high-frequent filter regeneration

related to CDC could decrease the reported fuel economies considerably. Future improvements in these combustion technologies may also reduce engine out PM emissions which can further reduce the regeneration frequency and benefit fuel economies.

For our simulations, hybridization lowers emissions (see Table 5), except for the estimated PM emissions from CDC; thus, hybridization may reduce aftertreatment device size and cost in general. However, hybridization involves engine start-stop cycling which can reduce exhaust temperatures and affect catalyst performance. Interestingly, while PFI and lean GDI exhaust temperatures were lower for the hybrid case in comparison to the non-hybrid case, for CDC and RCCI cases, a slight increase in exhaust temperatures was observed over the drive cycle due to hybridization (Figure 12). The slightly higher temperatures are likely due to the fact that electric motor operation reduces the low load engine operation which is most closely associated with the lowest exhaust temperatures from CDC and RCCI combustion. Thus, hybridization might provide an additional emission control benefit for CDC and RCCI engines by permitting a modest increase in the exhaust temperatures.

5. Conclusions

The results for a conventional vehicle powered by a lean GDI engine indicate that it would have significantly better drive cycle fuel economy than the PFI engine-powered vehicle for all drive cycles. Hybridization appears to further increase the benefits of lean GDI engines over PFI engines because it increases the percentage of time the engine can operate at high efficiency lean conditions. In addition to the fuel economy gains achieved for lean GDI through hybridization, engine-out emissions also improve dramatically. Notably, PM emissions for the hybrid are predicted to be reduced to well the Tier 3 Bin 30 standard. Furthermore, hybridization appears to decrease both NOx and HC emissions significantly. Lean NOx aftertreatment may become more challenging for GDI due to reduced exhaust temperatures.

In the present study, vehicles with RCCI-enabled engines are predicted to have the highest fuel economies for all drive-cycles for both non-hybrid and hybrid configurations. As with lean GDI, hybridization appears to increase opportunities for exploiting the efficiency benefits of RCCI operation. RCCI engine-out NOx emissions are inherently low and decrease dramatically with increased use of this mode allowed by hybridization. Even though the NOx levels are very low for RCCI, the NOx+NMOG Tier 3 Bin 30 regulation is still challenging to meet because of the high CO and HC emissions and low exhaust temperatures. The latter characteristic of RCCI is of particular concern because exhaust temperature were predicted to fall frequently below 200ºC, where catalytic oxidation of CO and HCs becomes difficult.

Low exhaust temperatures do not appear to be a major issue for engines operating in CDC mode, and thus catalytic oxidation of HCs and CO are not so challenging in this case. However, enhanced aftertreatment for controlling particulate and NOx emissions under lean conditions is more important for CDC and can result in added fuel penalties. Likewise, the relatively high temperatures and stoichiometric conditions in PFI engine exhaust makes it possible to rely on three-way catalyst technology for emissions control. However, the new NOx+NMOG emission regulation is so challenging (requiring >99% reduction efficiency), it seems likely that PFI engines will have a difficult time competing in future advanced vehicles.

Overall, advanced passenger car combustion engines (enabled for lean GDI, RCCI, or CDC) are expected to permit sizeable gains in fuel economy relative to current PFI engines. Utilizing these advanced combustion engines in hybrid vehicles appear to offer still greater fuel economy benefits. However, emissions aftertreatment is likely to become an important limiting factor, especially until more effective, low-temperature oxidation catalysts become available. So understanding the relationships between fuel economy and emission controls will be critical in the development of advanced combustion technologies that meet the new U.S. EPA Tier 3 Bin 30 emission regulations. In this context, the potential benefits of hybridization that permit engines to operate under more optimal and less variable conditions will be of paramount importance.

All the above results are preliminary and are based on hypothetical vehicles that have not been built or experimentally studied. While the general trends are expected to be correct, the authors acknowledge that experimental validation of these conclusions will be a critical step in the development of future passenger car technologies. In presenting these results, it is our intention to suggest promising directions for such experiments.

Acknowledgments

We are indebted to the Office of Vehicle Technologies in the U.S. Department of Energy for supporting this research. We are also grateful to our colleagues at ORNL, who contributed helpful suggestions and insights. Thanks also go to the reviewers for their time and effort.

This manuscript has been authored by UT-Battelle, LLC under Contract No. DE-AC05-00OR22725 with the U.S. Department of Energy. The United States Government retains and the publisher, by accepting the article for publication, acknowledges that the United States Government retains a non-exclusive, paid-up, irrevocable, world-wide license to publish or reproduce the published form of this manuscript, or allow others to do so, for United States Government purposes. The Department of Energy will provide

public access to these results of federally sponsored research in accordance with the DOE Public Access Plan (http://energy.gov/downloads/doe-public-access-plan).

Nomenclature

BSFC : Brake specific fuel consumption
CDC : Conventional diesel combustion
CIDI : Compression-ignition direct-injection
CO : Carbon monoxide
CO_2 : Carbon dioxide
DOC : Diesel oxidation catalyst
DPF : Diesel particulate filter
EGR : Exhaust gas recirculation
EPA : Environmental Protection Agency
FSN : Filter smoke number
FTP : Federal test procedure
GDI : Direct gasoline injection
HC : Unburned hydrocarbons
HCCI : Homogeneous charge compression ignition
HEV : Hybrid electrical vehicle
HWFET : Highway fuel economy test
LD : Light-duty
LNT : Lean NOx trap
LTC : Low-temperature combustion
NiMH : Nickel–metal hydride
NMOG : Non-methane organic gases
NO_x : Nitrogen oxides
O_2 : Oxygen
ORNL : Oak Ridge National Laboratory
PCCI : Partially-premixed charge compression ignition
PFI : Port fuel-injected
PM : Particulate matter
RCCI : Reactivity controlled compression ignition
SCR : Selective catalytic reduction
SI : Spark ignited
SOC : State of charge
TWC : Three-way catalyst
UDDS : Urban dynamometer driving schedule
US06 : US06 Supplemental federal test procedure

References

1. US DRIVE Advanced Combustion and Emission Control Technical Team Roadmap. http://www1.eere.energy.gov/vehiclesandfuels/pdfs/program/acec_roadmap_june2013.pdf. Accessed July 18th, 2014.

2. John B. Heywood, Internal Combustion Engine Fundamental. 1th ed. McGraw-Hill, Inc.; 1988.

3. Light-Duty Automotive Technology, Carbon Dioxide Emissions, and Fuel Economy Trends: 1975 Through 2013. http://www.epa.gov/fueleconomy/fetrends/1975-2013/420r13011.pdf. Accessed July 18th, 2014.

4. Chambon P, Huff S, Norman K, Edwards K et al. European lean gasoline direct injection vehicle benchmark. SAE Technical Paper 2011-01-1218, 2011, doi:10.4271/2011-01-1218..

5. Schwarz C, Schünemann E, Durst B, Fischer J et al. Potentials of the spray-guided BMW DI combustion system. SAE Technical Paper 2006-01-1265, 2006, doi:10.4271/2006-01-1265.

6. Queiroz C, Tomanik, E. Gasoline direct injection engines - a bibliographical review. SAE Technical Paper 973113, 1997, doi:10.4271/973113.

7. Kaul B, Finney C, Wagner R, Edwards M. Effects of external EGR loop on cycle-to-cycle dynamics of dilute SI combustion. SAE Int. J. Engines 7(2):606-614, 2014, doi:10.4271/2014-01-1236.

8. Kirwan J, Shost M, Roth G, Zizelman J. 3-Cylinder turbocharged gasoline direct injection: a high value solution for low CO_2 and NOx emissions. SAE Int. J. Engines 3(1):355-371, 2010, doi:10.4271/2010-01-0590.

9. Zhao F, Lai MC, Harrington DL. Automotive spark-ignited direct-injection gasoline engines. Progress in Energy and Combustion Science. 1999; 25(5):437-562.

10. Park C, Kim S, Kim H, Moriyoshi Y. Stratified lean combustion characteristics of a spray-guided combustion system in a gasoline direct injection engine. Energy 2012; 41(1):401-407.

11. Wang C, Xu H, Herreros JM, Wang J, Cracknell R. Impact of fuel and injection system on particle emissions from a GDI engine. Applied Energy 2014; 132:178-191.

12. Bonatesta F, Chiappetta E, La Rocca A. Part-load particulate matter from a GDI engine and the connection with combustion characteristics. Applied Energy 2014; 124:366-376.

13. Liang B, Ge Y, Tan J, Han X et al. Comparison of PM emissions from a gasoline direct injected (GDI) vehicle and a port fuel injected (PFI) vehicle measured by electrical low pressure impactor (ELPI) with two fuels: gasoline and M15 methanol gasoline. Journal of Aerosol Science 2013; 57:22-31.

14. Gao Z, Chakravarthy VK, Daw CS. Comparisons of the simulated emissions and fuel efficiencies of diesel and gasoline hybrid electric vehicles. Proc. IMechE - Part D: Journal of Automobile Engineering 2011; 225(7):944-959.

15. Gao Z, Kim M-Y, Choi J-S, Daw CS, Parks II JE, Smith DE. Cold-start emissions control in hybrid vehicles equipped with a passive adsorber for hydrocarbons and nitrogen oxides. Proc. IMechE - Part D: Journal of Automobile Engineering 2012; 226(10):1396-1407.

16. Johnson TV Review of diesel emissions and control. International Journal of Engine Research 2009; 10(5):275-285.

17. Gao Z, Daw CS, Wagner RM. Simulating study of premixed charge compression ignition on light-duty diesel fuel economy and emissions control. Spring Technical Meeting of the Central States Section of the Combustion Institute, Dayton, OH, USA, April 22–24, 2012

18. Curran S, Gao Z, Wagner R. Reactivity controlled compression ignition drive cycle emissions and fuel economy estimations using vehicle systems simulations with E30 and ULSD. SAE Int. J. Engines 7(2):902-912, 2014, doi:10.4271/2014-01-1324.

19. Dempsey AB, Walker NR, Gingrich E, Reitz RD. Comparison of low temperature combustion strategies for advanced compression ignition engines with a focus on controllability. Combustion Science and Technology 2013; 186(2):210-241.

20. Szybist J, Edwards K, Foster M, Confer K et al., Characterization of engine control authority on HCCI combustion as the high load limit is approached, SAE Int. J. Engines 6(1):553-568, 2013, doi:10.4271/2013-01-1665.

21. Wagner R, Green J, Dam T, Edwards K et al., Simultaneous low engine-out NOx and particulate matter with highly diluted diesel combustion. SAE Technical Paper 2003-01-0262, 2003, doi:10.4271/2003-01-0262.

22. Gao Z, Wagner RM, Sluder CS, Daw CS, Green Jr JB. Using a phenomenological computer model to investigate advanced combustion trajectories in a CIDI engine. Fuel 2011; 90(5):1907–1918.

23. Kokjohn SL, Hanson RM, Splitter DA, Reitz RD. Fuel reactivity controlled compression ignition (RCCI): a pathway to controlled high-efficiency clean combustion. International Journal of Engine Research 2011; 12(3):209-226.

24. Yang B, Yao M, Cheng WK, Li Y et al. Experimental and numerical study on different dual-fuel combustion modes fuelled with gasoline and diesel. Applied Energy 2014; 113:722-733.

25. Gao Z, Curran SJ, Daw CS, Wagner RM. Light-duty drive cycle simulations of diesel engine-out exhaust properties for an RCCI enabled vehicle. 8th U. S. National Combustion Meeting Organized by the Western States Section of the Combustion Institute, Utah, USA, May 19-22, 2013.

26. Splitter D, Hanson R, Kokjohn S, Reitz R. Reactivity controlled compression ignition (RCCI) heavy-duty engine operation at mid-and high-loads with conventional and alternative fuels. SAE Technical Paper 2011-01-0363, 2011, doi:10.4271/2011-01-0363.

27. Kokjohn S, Hanson R, Splitter D, Reitz R. Experiments and modeling of dual-fuel HCCI and PCCI combustion using in-cylinder fuel blending. SAE Int. J. Engines 2(2):24-39, 2010, doi:10.4271/2009-01-2647.

28. Curran S, Hanson R, Wagner R. Effect of E85 on RCCI performance and emissions on a multi-cylinder light-duty diesel engine. SAE Technical Paper 2012-01-0376, 2012, doi:10.4271/2012-01-0376.

29. Curran S, Hanson R, Wagner R. Reactivity controlled compression ignition (RCCI) combustion on a multi-cylinder light-duty diesel engine. International Journal of Engine Research 2012; 13(2):216-225.

30. Curran S, Szybist J, Wagner R. Reactivity controlled compression ignition performance with renewable fuels. ICEF2012-92192, Proceedings of the ASME 2012 Internal Combustion Engine Division Fall Technical Conference, Vancouver, BC, Canada, September 23-26, 2012.

31. Gao Z, Daw C, Wagner R, Edwards K, Smith D. Simulating the Impact of premixed charge compression ignition on light duty diesel fuel economy and emissions of particulates and NOx. Proc. IMechE - Part D: Journal of Automobile Engineering 2013; 227(1):31-51.

32. Argonne National laboratory. Autonomie. http://www.autonomie.net/. Accessed December 4th, 2014.

33. Gao Z, Conklin J, Daw C, Chakravarthy V. A proposed methodology for estimating transient engine-out temperature and emissions from steady state maps. International Journal of Engine Research 2009; 11(2):137-151.

34. Prikhodko V, Parks J, Pihl J, Toops T. Ammonia generation over TWC for passive SCR NOx control for lean gasoline engines. SAE Int. J. Engines 7(3):2014, doi:10.4271/2014-01-1505.

35. Hanson R, Curran S, Wagner R, Reitz R. Effects of biofuel blends on RCCI combustion in a light-duty, multi-cylinder diesel engine. SAE Int. J. Engines 6(1):488-503, 2013, doi:10.4271/2013-01-1653.

36. Curran S, Hanson R, Wagner R, Reitz R. Efficiency and emissions mapping of RCCI in a light-duty diesel engine. SAE Technical Paper 2013-01-0289, 2013, doi:10.4271/2013-01-0289.

37. Prikhodko V, Curran S, Barone T, Lewis S et al. Emission characteristics of a diesel engine operating with in-cylinder gasoline and diesel fuel blending. SAE Int. J. Fuels Lubr. 3(2):946-955, 2010, doi:10.4271/2010-01-2266.

38. West B, López A, Theiss T, Graves R et al. Fuel economy and emissions of the ethanol-optimized Saab 9-5 biopower. SAE Technical Paper 2007-01-3994, 2007, doi:10.4271/2007-01-3994.

39. Cho K, Han M, Wagner R, Sluder C. Mixed-source EGR for enabling high efficiency clean combustion modes in a light-duty diesel engine. SAE Int. J. Engines 1(1):457-465, 2009, doi:10.4271/2008-01-0645.

40. Argonne National laboratory. Advanced Powertrain Research Facility - Downloadable Dynamometer Database (D3). http://www.transportation.anl.gov/D3/. Accessed by July 18th, 2014.

41. Buchholz K. Ford gets smarter about hybrid technology with Fusion. http://articles.sae.org/6810/. Accessed December 4th, 2014.

42. Das S. Automotive System Cost Modeling Tool (ASCM). http://web.ornl.gov/sci/ees/etsd/cta/Auto%20System%20Cost%20Modeling%20Tool.pdf. Accessed July 18th, 2014.

43. V.Gopal, R, Rousseau, A. System analysis using multiple expert tools. SAE Technical Paper 2011-01-0754, 2011, doi:10.4271/2011-01-0754.

44. Kim N, Kwon J, and Rousseau A. Comparison of powertrain configuration options for plug-in HEVs from a fuel economy perspective. SAE Technical Paper 2012-01-1027, 2012, doi:10.4271/2012-01-1027.

45. Dempsey A, Curran S, Storey J, Eibl M et al. Particulate matter characterization of reactivity controlled compression ignition (RCCI) on a light duty engine. SAE Technical Paper 2014-01-1596, 2014, doi:10.4271/2014-01-1596.

46. DieselNet. http://www.dieselnet.com/standards/us/ld_t3.php#ftp. Accessed July 18th, 2014.

47. Prikhodko V, Curran S, Parks J, Wagner R. Effectiveness of diesel oxidation catalyst in reducing HC and CO emissions from reactivity controlled compression ignition. SAE Int. J. Fuels Lubr. 6(2):329-335, 2013, doi:10.4271/2013-01-0515.

This article citation: Gao Z et al. Drive cycle simulation of high efficiency combustions on fuel economy and exhaust properties in light-duty vehicles. Applied Energy 157 (2015) 762–776, http://dx.doi.org/10.1016/j.apenergy.2015.03.070

Appendix A

Components	Unit	Conv SI		Conv GDI	Conv CDC	Conv RCCI*	Split SI		Split GDI	Split CDC	Split RCCI*
		3.0Fusion	2.0Saab	2.0BMW	1.9GM	1.9 GM	2.5Fusion	2.0Saab	2.0BMW	1.9GM	1.9GM
Engine rated power	kW	136	112	125	114	114	116	112	125	114	114
Motor rated power	kW	0	0	0	0	0	36	36	36	36	36
Generator rated power	kW	0	0	0	0	0	36	36	36	36	36
High-voltage battery rated power	kW	0	0	0	0	0	36	36	36	36	36
Engine body	kg	286	235	263	194	194	243	235	263	194	194
Fuel tank	kg	40	40	40	40	40	40	40	40	40	40
Stored fuel	kg	28	28	28	28	28	28	28	28	28	28
Aftertreatment system	kg	30	30	60	60	60	30	30	60	60	60
12V battery	kg	22	22	22	22	22	0	0	0	0	0
High voltage battery	kg	0	0	0	0	0	66	66	66	66	66
Motor controller	kg	0	0	0	0	0	46	46	46	46	46
Motor	kg	0	0	0	0	0	43	43	43	43	43
Alternator/Generator	kg	6.5	6.5	6.5	6.5	6.5	43	43	43	43	43
Gearbox	kg	75	75	75	75	75	70	70	70	70	70
Final drive	kg	32	32	32	32	32	32	32	32	32	32
Wheel	kg	100	100	100	100	100	100	100	100	100	100
Clutch/Torque converter	kg	25	25	25	25	25	0	0	0	0	0
Starter	kg	3	3	3	3	3	3	3	3	3	3
Mechanical acessory	kg	35	35	35	38	38	30	30	30	33	33
Electrical acessory	kg	18	18	18	18	18	36	36	36	36	36
Accessory related HECC		0	0	0	0	50	0	0	0	0	50
Glider mass	kg	865	865	865	865	865	868	868	868	868	868
Curb Vehicle Weight	kg	1565	1515	1572	1507	1557	1678	1670	1728	1662	1712
Cargo & Driver Mass	kg	136	136	136	136	136	136	136	136	136	136
Gross Vehicle Weight	kg	1701	1651	1708	1643	1693	1814	1806	1864	1798	1848

Note: The mass weight of engine, motor, generator and battery are determined based on a function of the component rate powers; gasoline engine mass=2.1*engine power; diesel engine mass=1.7*engine power; high-voltage battery mass=1.82*battery power; motor mass=1.2*motor power.